iScience

CellPress
OPEN ACCESS

Article

A natural product targets BRD4 to inhibit phase separation and gene transcription

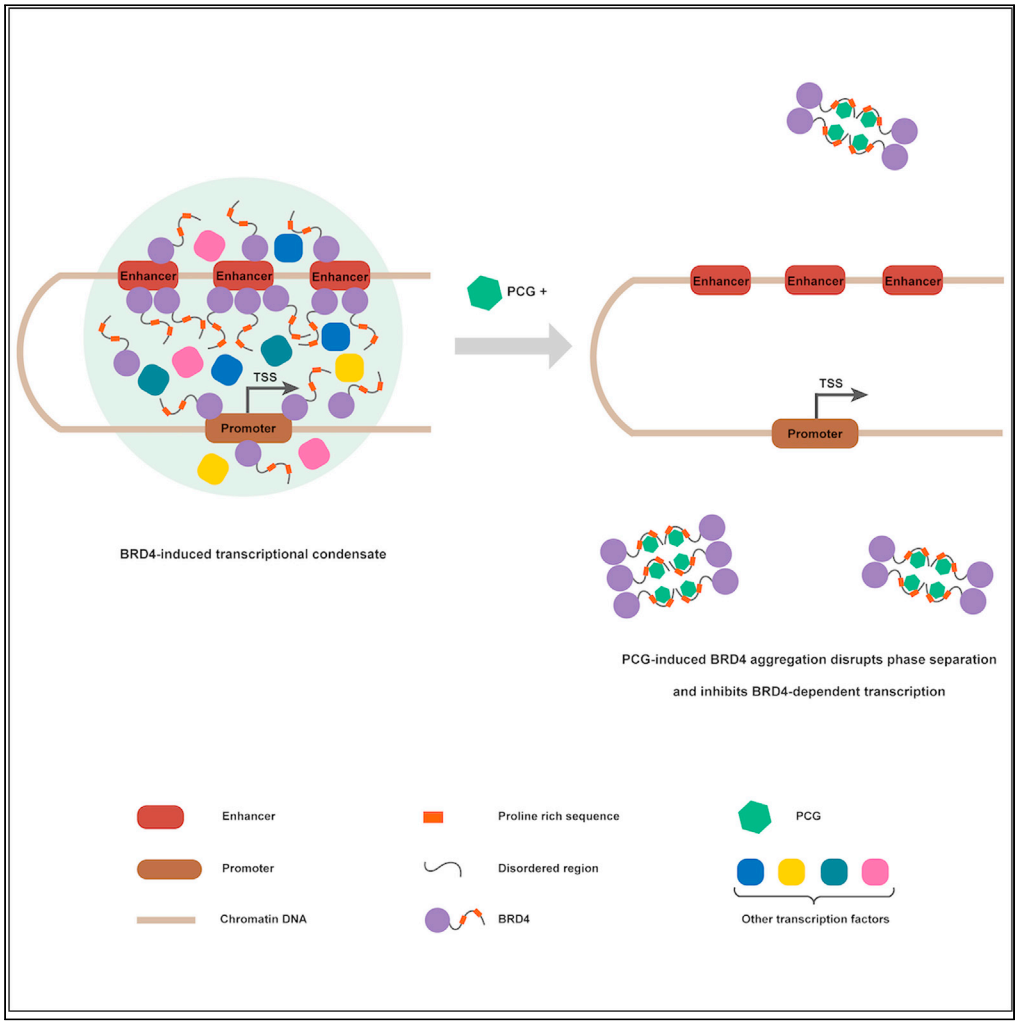

Cong Wang, Huasong Lu, Xiangzhong Liu, ..., Haifeng Chen, Yuhua Xue, Qiang Zhou

haifeng@xmu.edu.cn (H.C.)
xueyuhua@xmu.edu.cn (Y.X.)
qzhou@berkeley.edu (Q.Z.)

Highlights

Natural product PCG induces aggregation of BRD4 but no other BET family proteins

PCG targets proline-rich sequences in BRD4 intrinsically disordered region

PCG turns phase-separated BRD4 into static aggregates *in vivo* and *in vitro*

The PCG-induced aggregation inhibits BRD4-dependent transcription

Wang et al., iScience *25*, 103719
January 21, 2022
https://doi.org/10.1016/j.isci.2021.103719

iScience

CellPress
OPEN ACCESS

Article

A natural product targets BRD4 to inhibit phase separation and gene transcription

Cong Wang,[1,2,4] Huasong Lu,[2,3,4] Xiangzhong Liu,[1] Xiang Gao,[1] Wenjing Tian,[1] Haifeng Chen,[1,*] Yuhua Xue,[1,*] and Qiang Zhou[2,5,*]

SUMMARY

The BET-bromodomain protein BRD4 uses two bromodomains to target acetyl-histones and other domains to recruit P-TEFb and other transcription factors to stimulate transcription of proto-oncogenes and key cell identity genes. Recent studies show that its ability to form phase-separated condensates that cluster preferentially at the super-enhancer regions of target genes is key for BRD4 to exert its functions. Here, we describe the identification of a natural product called PCG from *polygonum cuspidatum* Sieb.et Zucc., a traditional Chinese medicinal herb, that directly binds to BRD4. This binding inhibits BRD4 phase separation, turns dynamic BRD4 nuclear condensates into static aggregates, and effectively shuts down transcription of BRD4-dependent genes. Thus, through PCG we have discovered a BET inhibitor that not only selectively targets BRD4 but also works by suppressing phase separation, a mechanism of action that is different from those of the other known BET inhibitors.

INTRODUCTION

BRD4 is a well-known transcriptional co-activator and epigenetic reader of acetylated chromatin (Devaiah et al., 2016). It is a promising drug target for treating various diseases ranging from cancer to HIV-1 infection. Recent studies show that BRD4, together with MED1, preferentially cluster at super-enhancers of proto-oncogenes and key cell identity genes (Loven et al., 2013) through forming phase-separated condensates that recruit components of the transcriptional machinery to drive gene expression (Sabari et al., 2018). BRD4 uses its two N-terminal bromodomains (BDs) to bind to acetylated histones, the central extraterminal (ET) domain to interact with diverse transcriptional regulators (Belkina and Denis, 2012; Shi and Vakoc, 2014), and the C-terminal P-TEFb-interacting domain (PID) to recruit the general transcription factor P-TEFb to the target genes to stimulate transcriptional elongation (Jang et al., 2005; Yang et al., 2005).

Although the BRD4-P-TEFb interaction is required to activate expression of many cellular genes, it is inhibitory to HIV-1 transcription and latency reversal, which depend on the viral-encoded Tat protein. BRD4 has been shown to inhibit Tat-transactivation by competing with Tat for binding to P-TEFb, which interferes with the more efficient Tat-mediated P-TEFb recruitment route used by HIV for maximal transcription and latency reversal(Bacon and D'Orso, 2019; Yang et al., 2005; Zhou et al., 2012).

Given its importance in regulating cellular and HIV-1 transcription, targeting BRD4 can be an effective strategy to combat cancer and control HIV latency. To this end, a number of BRD4 inhibitors (called the BET inhibitors or BETi) have been developed and a few tested in clinical trials (Bechter and Schoffski, 2020). The vast majority of them work by disrupting the interaction between the BRD4 BDs and acetyl-lysines. However, these drugs can also act on other BET family members BRD2, BRD3, and BRDT (Chiang, 2016), which all contain the conserved BDs but lack the C-terminal PID and thus cannot functionally substitute for BRD4 in recruiting P-TEFb. In addition, some of the inhibitors affect gene transcription by other unrelated means (Bai et al., 2017; Cai et al., 2011; Lu et al., 2015). The lack of selectivity against BRD4 and the pleiotropic effects of the available BET inhibitors have limited their use in treating BRD4-driven diseases.

Previously, in an effort to identify latency-reversing agents (LRAs) that can be used to reactivate latent HIV-1 reservoirs for subsequent eradication, we isolated a natural product called PCG (procyanidin C-13,3′,3″-tri-O-gallate; previously called REJ-C1G3) from *polygonum cuspidatum* Sieb.et Zucc., a traditional Chinese

[1]State Key Laboratory of Cellular Stress Biology Fujian Provincial Key Laboratory of Innovative Drug Target Research, School of Pharmaceutical Sciences, Xiamen University, Xiang'an South Road, Xiamen, Fujian 361102, China

[2]Department of Molecular and Cell Biology, University of California, Berkeley, CA 94720, USA

[3]Life Sciences Institute, Zhejiang University, Hangzhou 310058, China

[4]These authors contributed equally

[5]Lead contact

*Correspondence: haifeng@xmu.edu.cn (H.C.), xueyuhua@xmu.edu.cn (Y.X.), qzhou@berkeley.edu (Q.Z.)

https://doi.org/10.1016/j.isci.2021.103719

medicinal herb, that can efficiently reverse HIV-1 latency (Wang et al., 2015). PCG was found to preferentially activate the Tat-dependent HIV-1 transcription. Because BRD4 is a known inhibitor of Tat (Yang et al., 2005), we investigated the possibility that PCG stimulates Tat-transactivation through antagonizing BRD4's function. Indeed, our data indicate that PCG can directly target BRD4 through binding to the proline-rich sequences that are only present in BRD4 but not other BET family members. This binding induces misfolding and aggregation of BRD4, and prevents the formation of phase-separated BRD4 droplets *in vitro*. Inside the cell nucleus, PCG turns the dynamic BRD4 nuclear condensates into static aggregates, which in turn inhibits transcription of BRD4-dependent genes. Thus, as a medicinal herb-derived natural product, PCG displays the potential as a selective BRD4 inhibitor that works by inhibiting phase separation and can substitute for the conventional BET inhibitors in treating human diseases.

RESULTS

PCG treatment causes BRD4 to disappear from SDS-gel

We previously reported that PCG can reactivate HIV-1 from latency in a Tat-dependent manner (Wang et al., 2015). However, the underlying mechanism was largely unclear. In an effort to identify the potential target of PCG, we first performed SDS-PAGE followed by immunoblotting analysis to investigate whether exposure to the drug by HeLa cells could affect the cellular levels of P-TEFb and its various associated proteins that collectively form a network of P-TEFb complexes important for HIV-1 transcriptional control and latency (Lu et al., 2013). As a positive control, JQ1 and prostratin, two well-characterized HIV-1 latency-reversing agents (LRA(Williams et al., 2004; Bartholomeeusen et al., 2012)), were used. While the levels of CDK9, CycT1, the 7SK snRNP components HEXIM1, LARP7 and MePCE, and the SEC subunits AFF1, AFF4, and ELL2 remained mostly unchanged in whole cell extracts (WCE) after the treatment, the BRD4 level decreased dramatically (Figure 1A). Because BRD4 and its inhibition of Tat-transactivation is known as a major impediment to latency reactivation (Banerjee et al., 2012; Bartholomeeusen et al., 2012; Li et al., 2013), the induced loss of BRD4 explains the previously reported positive effect of PCG on HIV-1 latency reversal (Wang et al., 2015).

Interestingly, when cells were treated with increasing concentrations of PCG, BRD4 first shifted upward in an SDS-PAGE gel starting at 15 μM PCG and then completely disappeared at 150 μM PCG (Figure 1B). The disappearance of BRD4 was detected as early as 2 h after the start of the treatment (Figure S1). This effect was at the protein level as the BRD4 mRNA level was little affected by PCG (75 μM) or two well-studied BRD4-targeting drugs, JQ1 and ARV825, at concentrations (1 μM and 0.2 μM, respectively) known to be effective (Figure 1C). JQ1 specifically binds and blocks the interactions of the BRD4 bromodomains with acetylated histones (Delmore et al., 2011), while ARV825 is known to recruit BRD4 to the E3 ubiquitin ligase cereblon to cause proteasomal degradation (Lu et al., 2015). As expected, the cellular BRD4 protein level was unaffected by DMSO and JQ1, but significantly reduced by ARV825 (Figure 1C). In comparison, the exposure to PCG caused most BRD4 to disappear while the remaining residual amount to display an upshift in the SDS-gel (Figure 1C).

PCG causes BRD4 to become SDS-insoluble

One possible reason for the observed loss of BRD4 is that PCG induces proteasomal degradation of the protein. To test this possibility, we pretreated cells with the proteasome inhibitor MG132 to see whether this would prevent PCG from causing BRD4 to disappear from the SDS-gel. While MG132 efficiently suppressed the ARV825-induced BRD4 degradation as expected, it surprisingly produced no effect on the PCG-mediated loss of BRD4 (Figure 1D).

This unexpected result prompted us to investigate whether PCG also made BRD4 to disappear in cells or only in the SDS-gel. To this end, we first performed an anti-BRD4 immunofluorescence staining of HeLa cells treated with PCG or the controls DMSO and ARV825. The result clearly shows that compared to cells incubated with DMSO, the BRD4 fluorescence signal did not display any noticeable loss in PCG-treated cells, whereas it was largely gone upon the exposure to ARV825 (Figure 1E).

To further investigate the reason behind the PCG-induced loss of BRD4 in the SDS-gel, we added 8M urea, a chaotropic compound known to destroy secondary protein structure and bring otherwise insoluble proteins into solution, into the cell lysis buffer. While WCE obtained with the urea-free lysis buffer still showed no BRD4 in the SDS-gel, the urea-containing buffer caused BRD4 to reappear (Figure 1F). Taken together, these results indicate that rather than causing BRD4 protein to degrade, PCG likely induced misfolding and

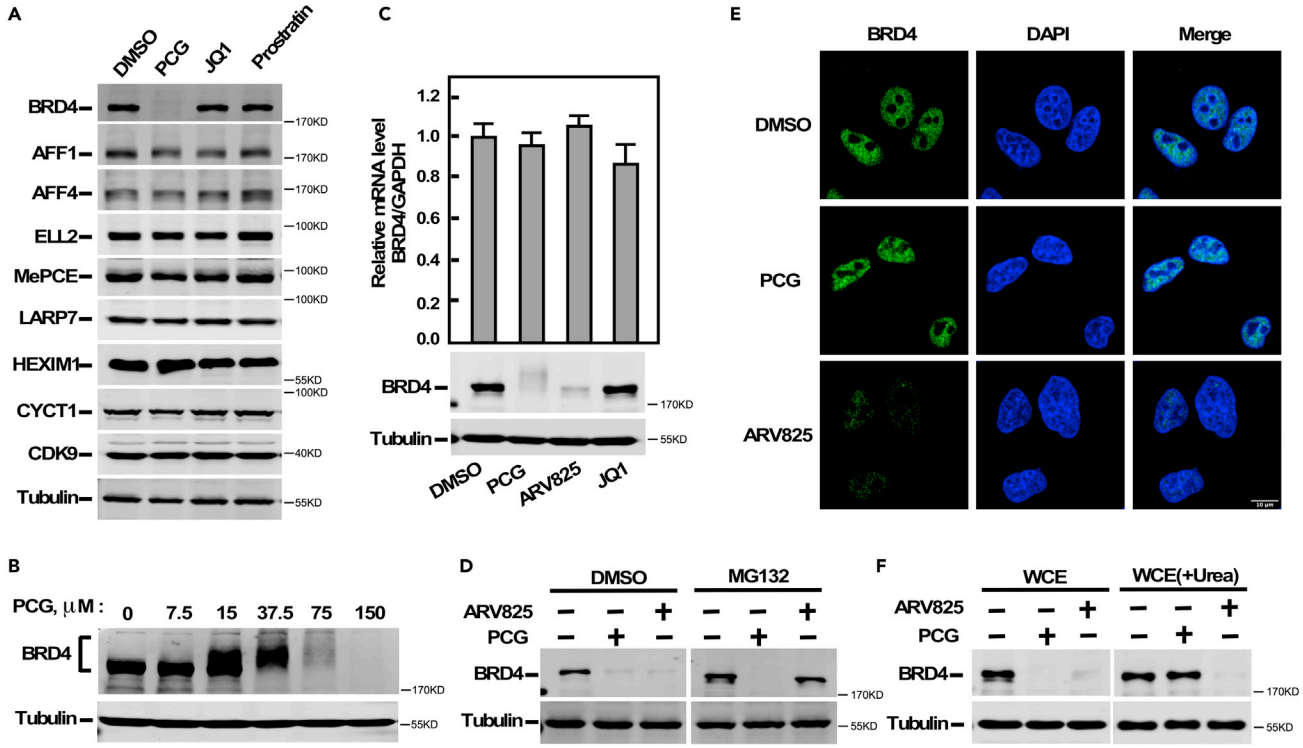

Figure 1. PCG treatment does not cause BRD4 degradation but to make the protein SDS-insoluble

(Aand B) HeLa cells were treated for 6 h with DMSO, 1 μM JQ1, 2.5 μM prostratin, and 75 μM (A) or the indicated concentrations (B) of PCG. Whole cell lysates (WCE) were examined by SDS-PAGE followed by western blotting for the proteins labeled on the left.

(C) HeLa cells were treated for 6 h with DMSO, 1 μM JQ1, 0.2 μM ARV825, and 75 μM PCG. Top: The mRNA levels of BRD4 were analyzed by RT-qPCR, normalized to those of GAPDH and shown, with the level in DMSO-treated cells set to 1.0. The error bars represent mean ± SD from three independent measurements. Bottom: BRD4 and α-Tubulin in WCE of the treated cells were detected by western blotting.

(D) HeLa cells were pretreated with DMSO or 20 μM MG132 for 2 h and then treated with 75 μM PCG or 0.2 μM ARV825 for 6 h. Western blotting was performed afterwards to detect BRD4 and α-Tubulin in WCE.

(E) HeLa cells were treated with DMSO, 75 μM PCG, or 0.2 μM ARV825 for 6 h and then analyzed by immunofluorescence (IF) with the rabbit anti-BRD4 antibody and Alexa Fluor 488-conjugated goat anti-rabbit secondary antibody. DNA was counterstained with DAPI. Scale bar 10μm.

(F) HeLa cells were treated the same way as in E and then lysed with either normal cell lysis buffer or the buffer containing 8 M urea. WCE were prepared and analyzed as in (D)

aggregation of BRD4, which made the protein insoluble even in the presence of a strong detergent such as SDS.

PCG directly binds and causes misfolding and aggregation of BRD4

Did PCG directly bind to BRD4 to induce aggregation or initiate a signaling pathway in cells that indirectly made BRD4 SDS-insoluble? To answer this question, we affinity-purified Flag-tagged BRD4 (F-BRD4) from cells (Figure 2A, bottom) and incubated it with PCG *in vitro*. Similar to the scenario involving treatment of living cells with PCG, purified F-BRD4 became SDS-insoluble after the incubation (Figure 2A, top), indicating that PCG could directly bind to and induce misfolding and aggregation of BRD4.

Furthermore, when WCE were incubated with increasing concentrations of PCG *in vitro*, BRD4 first displayed an upshift in the SDS-gel and then disappeared at higher drug concentrations (Figure 2B). This latter effect could be completely reversed by the addition of 8 M urea into the WCE (Figure 2C). Together, these data indicate that PCG directly targets BRD4 to cause misfolding and aggregation.

Proline-rich sequences in BRD4 are required for PCG-induced BRD4 aggregation

When cells expressing the N-terminal half of BRD4 (F-BRD4-1-700) that contains the dual bromodomains (BD1 & BD2) and the extraterminal (ET) domain (Figure 3A) were incubated with PCG, this BRD4 fragment

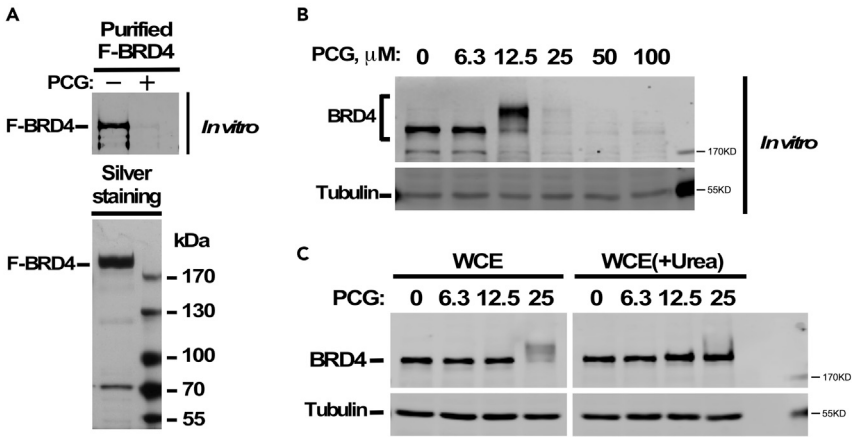

Figure 2. PCG directly binds and causes misfolding and aggregation of BRD4

(A) F-BRD4 was affinity-purified from transfected 293T cells and examined by SDS-PAGE followed by silver-staining (bottom). F-BRD4 was then incubated with 50 μM PCG for 10 min at room temperature and examined by SDS-PAGE followed by anti-Flag western blotting (WB; top).

(B)Whole cell extracts (WCE) of HeLa cells were incubated with the indicated concentrations PCG for 10 min at room temperature and then analyzed by WB for the proteins labeled on the left.

(C) Urea (8 M) was added or not into the WCE from B, which were then analyzed by SDS-PAGE/WB as in (B)

was completely insensitive to the drug (Figure 3A). In contrast, the C-terminal half (F-BRD4-701-1362), which contains stretches of proline-rich sequences and the PID (P-TEFb-interacting domain) at the very end, displayed the same PCG-induced misfolding and aggregation as shown by the full-length protein.

To determine which part of the BRD4 C-terminal half was required for PCG to exert this effect, a series of C-terminally truncated BRD4 that all contain the intact C-terminus but progressively shortened N-termini were expressed in HeLa cells and the WCE were incubated with PCG. Compared to aa701-1362, which was highly responsive to PCG, aa1001-1362 was only slightly and aa801-1362 and aa901-1362 were partially affected by the drug (Figure 3B). In contrast, aa1101-1362 and aa1208-1362 were completely non-responsive. These results suggest that the region between aa701 and 1100 in BRD4 is likely required for PCG to target and induce BRD4 aggregation. Consistent with this prediction, when isolated from the rest of BRD4, aa701-1100 alone became SDS-insoluble upon exposure to PCG both *in vivo* (Figure 3C) and *in vitro* (Figure 3D).

A close examination of the BRD4 sequence from aa701 to 1100 reveals two prominent proline-rich sequences termed P1 (aa751-800) and P2 (aa951-1031) (Figure 3E). When both P1 and P2 were simultaneously deleted (ΔP1&P2), the PCG-induced BRD4 aggregation was effectively blocked *in vitro* (Figure 3F) and *in vivo* (Figure 3G). Compared to WT BRD4, the single deletion of P1 (ΔP1) or P2 (ΔP2) allowed BRD4 to respond to PCG partially (Figure 3F).

Different from BRD4, the other BET family members including BRD2, BRD3, and BRDT only contain the conserved BD and ET domains but lack the proline-rich segments (Figure 3H, bottom). Importantly, only BRD4 but not other BET family members responded to the PCG treatment (Figure 3H). This result supports the notion that the proline-rich sequences are required for PCG to induce misfolding and aggregation of BRD4.

Proline-rich sequences in BRD4 are required for PCG to inhibit BRD4 droplet formation *in vitro*

The intrinsically disordered region (IDR) of BRD4, where the two low-complexity P1 and P2 sequences reside, has been shown to enable BRD4 to undergo liquid–liquid phase separation (LLPS) at super-enhancers(Sabari et al., 2018). In light of the above observations that PCG directly targets the proline-rich sequences in P1 and P2 to induce misfolding of BRD4, we investigated whether PCG could affect phase separation by BRD4.

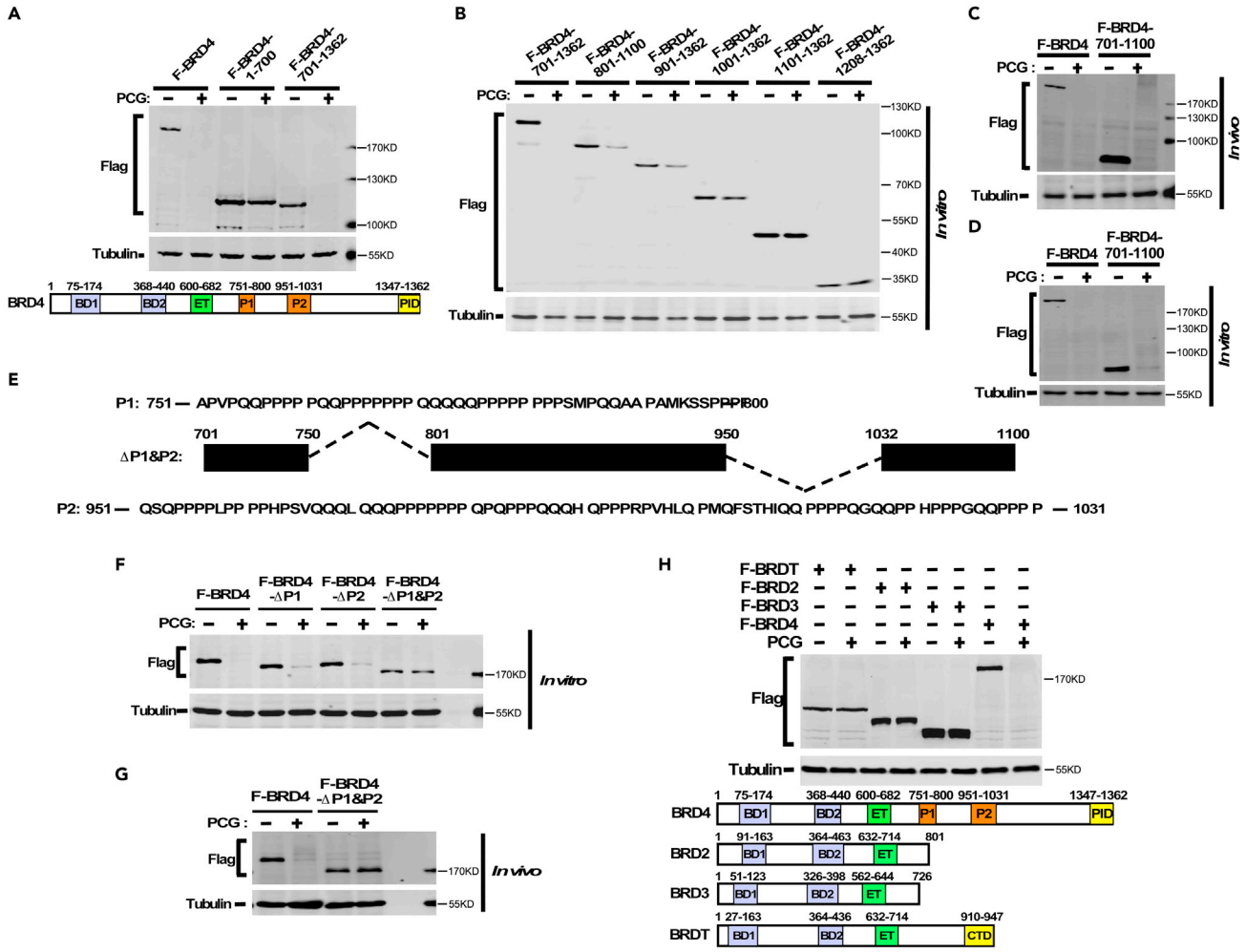

Figure 3. Proline-rich segments in BRD4 are required for PCG-induced BRD4 aggregation

(A, C, G, and H) HeLa cells were transfected with plasmids expressing the indicated full-length or truncated F-BRD4 (A, C, & G), or the indicated Flag-tagged BET family members. 48 h later, the cells were treated with DMSO or 75 μM PCG for 6 h. Whole cell extracts (WCE) were prepared and analyzed by anti-Flag western blotting (WB). A diagram of the various domains/segments and their positions in BRD4 is shown at the bottom of (A). BD1 & 2: Bromodomains 1 & 2. ET: Extraterminal domain. P1 & P2: Proline-rich segments. PID: P-TEFb-interaction domain.

(B, D, and F) WCE were prepared from HeLa cells transfected with plasmids expressing the indicated full-length and truncated F-BRD4, incubated with 50 μM PCG for 10 min at room temperature, and then analyzed by WB.

(E) The sequences and positions of two proline-rich segments in BRD4 as well as the structure of BRD4(ΔP1&P2), in which the two proline-rich segments are deleted, are shown.

To this end, we purified from *E. coli* recombinant EGFP fusion proteins containing either WT BRD4 IDR (aa721-1351) or a mutant IDR lacking P1 and P2 (ΔP1&P2) (Figure 4A). When incubated with PCG, the WT but not the mutant fusion protein became SDS-insoluble as predicted (Figure S2A). In the absence of any crowding agents, both fusion proteins readily formed droplets in a concentration-dependent manner, with EGFP-IDR(ΔP1&P2) producing bigger size droplets compared to EGFP-IDR(WT) under the same conditions (Figure 4B). The droplets could be easily disrupted by 10% 1,6-hexanediol, which is routinely used to inhibit LLPS (Figure S2B) (Molliex et al., 2015; Strom et al., 2017).

Importantly, adding PCG into the EGFP-IDR(WT) solution dose-dependently inhibited the formation of small spherical droplets and led to the production of protein aggregates of irregular shapes and sizes (Figure 4C). Consistent with the above demonstrations that PCG depended on the poly-proline sequences in P1 and P2 to target BRD4, the incubation of PCG with EGFP-IDR(ΔP1&P2) failed to induce protein aggregation (Figure 4C).

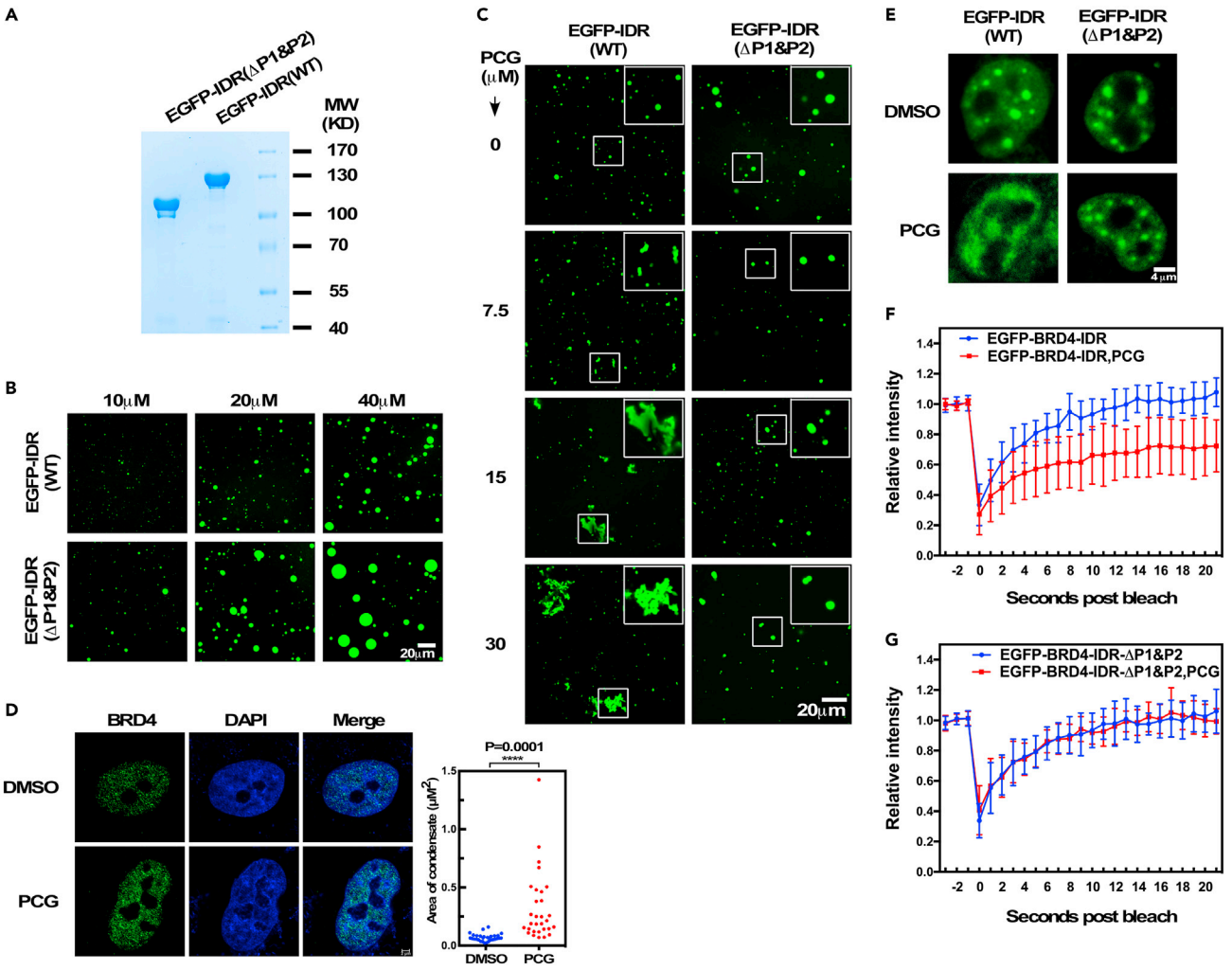

Figure 4. PCG converts dynamic BRD4 phase separation into static aggregation

(A) EGFP-IDR(WT) and EGFP-IDR(ΔP1&P2) were expressed in and purified from recombinant *E. coli* and examined by SDS-PAGE followed by Coomassie blue staining.

(B) Solutions containing either EGFP-IDR(WT) or EGFP-IDR(ΔP1&P2) at the indicated protein concentrations in droplet formation buffer were trapped between coverslips and examined with a microscope under fluorescent light. Representative images of the formed droplets are shown. Scale bar 20 μm.

(C) Solutions containing EGFP-IDR(WT) or EGFP-IDR(ΔP1&P2) were allowed to form droplets and then incubated with the indicated concentrations of PCG at room temperature for 10 min. The samples were examined by fluorescence microscopy as in (B). The inset at the upper right corner of each image is a 2x enlargement of the boxed area in the same image. Scale bar 20 μm.

(D) HeLa cells were treated with DMSO or PCG for 6 h. Shown are representative images of immunofluorescence staining with anti-BRD4 antibody and Alexa Fluor 488-conjugated goat anti-rabbit secondary antibody. DNA was counterstained with DAPI. Scale bar 4 μm. Quantification of the sizes of BRD4 puncta by ImageJ is shown on the right. Six puncta were quantified for each cell, and 5 cells in each group were quantified. Each dot represents a punctum, $n = 30$ in each group. The statistical significance is calculated by two-tailed Student's *t*-test.

(E) HeLa cells expressing EGFP-IDR(WT) or EGFP-IDR(ΔP1&P2) were incubated with either DMSO or 50 μM PCG for 10 min and then examined by fluorescence microscopy and representative cell images are shown. Scale bar 4 μm.

(F and G) The same cells analyzed in E were subjected to FRAP analysis of the EGFP-IDR(WT) and EGFP-IDR(ΔP1&P2) puncta and shown are fluorescence recovery plots. The puncta were photobleached at t = 0 s. The intensities at the spots were normalized to pre-bleach intensities and shown at various time points after the bleach as mean ± SD (N = 10). See Figure S4 for statistical analyses.

PCG turns dynamic BRD4 nuclear condensates into static aggregates *in vivo*

Next, we performed anti-BRD4 immunofluorescence (IF) staining to examine how LLPS by endogenous BRD4 could be affected by PCG. In the absence of PCG, BRD4 displayed small discrete puncta in the nucleus (Figure 4D) just as reported previously (Sabari et al., 2018). However, upon exposure to PCG, these

puncta coalesced into bigger and brighter spots that displayed largely irregular shapes (Figure 4D). A similar PCG-induced change was also observed during anti-Flag IF staining of HeLa cells expressing WT F-BRD4 (Figure S2C). In contrast, cells expressing F-BRD4-ΔP1&P2 displayed no significant change after the drug treatment (Figure S2C).

To rule out the possibility that this PCG-induced change in distribution of WT BRD4 was the result of cell fixation process in IF, we also examined the impact of PCG on distributions of EGFP-IDR(WT) and EGFP-IDR(ΔP1&P2) in living cells. The data indicate that while the two fusion proteins displayed a similar pattern of nuclear puncta distribution when exposed to DMSO, they responded very differently to PCG (Figure 4E). As predicted, PCG did not alter the distribution pattern of EGFP-IDR(ΔP1&P2), but it caused the sharply focused EGFP-IDR(WT) puncta to disperse into wider and more defused areas in the nucleus (Figure 4E).

An important feature of phase-separated condensates *in vivo* is their ability to undergo dynamic reorganization and exchange with the environment (Hyman et al., 2014). To investigate how PCG would affect the BRD4 condensates to display such a feature, we performed fluorescence recovery after photobleaching (FRAP) in HeLa cells expressing EGFP-IDR(WT) or EGFP-IDR(ΔP1&P2). For the EGFP-IDR(WT) condensates, PCG significantly reduced the extent of recovery after photobleaching when compared to DMSO, with the plateau intensities of EGFP-IDR(WT) in the presence of DMSO and PCG reaching 1.049 and 0.721, respectively (Figures 4F and 4G&Figure S3). In contrast, the EGFP-IDR(ΔP1&P2) condensates showed a similarly efficient recovery after both treatments, with the plateau intensities of EGFP-IDR(ΔP1&P2) in the presence of DMSO and PCG at 1.025 and 1.031, respectively. Together, these results indicate that PCG targets BRD4 to turn the highly dynamic BRD4 nuclear condensates into static aggregates *in vivo*.

PCG-induced BRD4 aggregation inhibits transcription of BRD4-dependent genes

The activity of super-enhancers depends on the condensates of BRD4 and Mediator, which compartmentalize and concentrate the transcription apparatus to promote expression of key cell identity genes (Sabari et al., 2018). One such gene is *MYC*, which stimulates tumor cell growth and proliferation through amplification of gene transcription (Kress et al., 2015). Given its importance in tumorigenesis, the expression of *MYC* has been studied extensively in a wide range of tumors and shown to be suppressed by JQ1 (Delmore et al., 2011; Loven et al., 2013; Mertz et al., 2011; Ott et al., 2012; Zuber et al., 2011), a well-characterized BET inhibitor that disrupts super-enhancers by displacing BRD4 from acetylated chromatin(Filippakopoulos et al., 2010; Loven et al., 2013).

To examine whether the PCG-induced BRD4 aggregation would affect the expression of *MYC* in cancer cells, MDA-MB-231, a triple-negative breast cancer cell line that is highly sensitive to JQ1(Bai et al., 2017; Shu et al., 2016) and addictive to *MYC* overexpression (Lao-On et al., 2020; Xu et al., 2010), was treated with PCG or JQ1, which served as a positive control. Like the situation in Hela cells, PCG also caused BRD4 aggregation in MDA-MB-231 cells (Figure S4). Analysis of mRNA production by RT-qPCR showed that not only JQ1 but also PCG markedly reduced *MYC* expression (Figure 5A). Further analysis by ChIP-qPCR indicates that the diminished *MYC* expression correlated with a significant PCG- or JQ1-induced decrease in the occupancy of BRD4 across the *MYC* locus (Figure 5B). The decrease was more prominent at the upstream enhancer (positions A & B) and a promoter-proximal location (position C) than at the downstream regions (positions D, E, & F).

In addition to *MYC*, we also tested the effect of PCG on the expression of several other key growth-regulating genes including *CDCA5*, *CDC6*, *RRM2*, and *MCM3* in MDA-MB-231 cells. These genes have enhancers that display super-enhancer-like functional properties and are enriched in and dependent on BRD4 for efficient transcription (Zanconato et al., 2018). Similar to the *MYC* situation, mRNA production from these genes was inhibited by not only JQ1 but also PCG (Figure 5C). Furthermore, just like the observation made at the *MYC* locus, the occupancy of BRD4 at the enhancer region of these genes also showed a significant drop after the treatment with PCG or JQ1 (Figure 5D). Based on these results, we conclude that the PCG-induced BRD4 aggregation is as effective as the BET inhibitor JQ1 in inhibiting transcription of the BRD4-dependent genes.

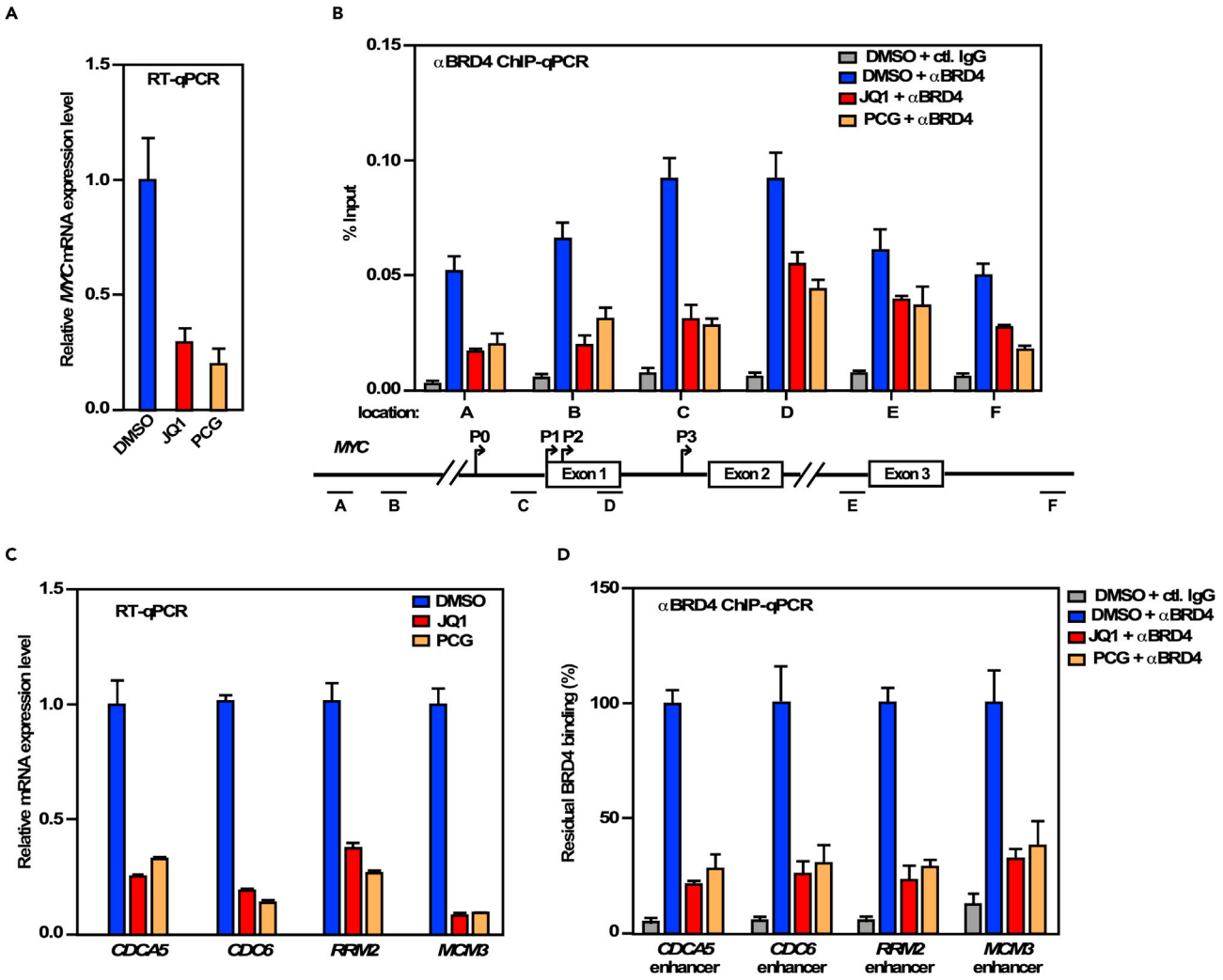

Figure 5. PCG-induced BRD4 aggregation inhibits transcription of BRD4-driven genes

(A and C) MDA-MB-231 cells were treated for 24 h with DMSO, 1 μM JQ1, or 75 μM PCG and subjected to RT-qPCR analyses to detect the mRNA levels of *MYC* (A) or the indicated genes. The signals were normalized to the mRNA levels of GAPDH and shown.

(B and D) MDA-MB-231cells were treated as in A and subjected to ChIP-qPCR analyses to assess the occupancy of BRD4 at the various locations across the *MYC* locus (B, bottom) or the enhancer region of the indicated genes (D). The signals were normalized to the input DNA and shown. All error bars represent mean ± SD from three independent measurements.

DISCUSSION

Multiple studies have shown that BRD4 serves as a chromatin adaptor and regulates the expression of key proto-oncogenes and cell identity genes in part through forming phase-separated condensates that cluster preferentially at the super-enhancer regions of these genes (Chapuy et al., 2013; Loven et al., 2013). These functions make BRD4 a promising therapeutic target in a number of diseases ranging from HIV/AIDS to cancer (Banerjee et al., 2012; Li et al., 2013; Wu et al., 2020). In clinical trials as well as in laboratory research, the function of BRD4 is routinely inhibited by a group of compounds collectively referred to as the BET inhibitors (BETi(Liu et al., 2017)), which work by disrupting the interactions between the bromodomains of BRD4 and acetyl-lysines of histones. Notably, these compounds do not directly act on the BRD4 phase separation process per se. Moreover, they display little selectivity between BRD4 and the rest of the BET family (Chiang, 2016), which all contain bromodomains but lack the P-TEFb-interacting domain such as the one present at the very C-terminus of BRD4 (Jang et al., 2005; Yang et al., 2005).

In this study, we find that PCG, a natural product derived from a traditional Chinese medicinal herb, can directly bind to BRD4 to induce aggregation that makes the protein insoluble even in a strong detergent such as SDS. This effect directly inhibits BRD4 phase separation, turns dynamic BRD4 nuclear condensates into static aggregates, and effectively shuts down transcription of BRD4-dependent genes. Notably, PCG affected the proliferation of HeLa and MDA-MB-231 cells only at high concentration ($\geq$100 μM) (Figure S5). Our further analyses have identified two proline-rich segments (P1 & P2) in BRD4 as the direct target of PCG. Importantly, these two segments are unique to BRD4 and completely missing in the rest of the BET family. Thus, through PCG we have discovered a BETi that not only selectively targets BRD4 but no other BET family members but also works by directly suppressing phase separation, a mechanism of action that is very different from those of other known BETi.

PCG belongs to the procyanidin class of polyphenols. These compounds are known to bind to proline-rich proteins, but the underlying mechanisms are complex (Fraga et al., 2010). Previous reports have shown that the polyphenol compound EGCG preferentially binds to hydrophobic, unfolded polypeptides to induce aggregation (Ehrnhoefer et al., 2008; Palhano et al., 2013). It is interesting to note that at the concentrations of PCG that caused BRD4 aggregation, the solubility of SET1A, a component of the histone lysine methyltransferase complex, was little affected (Figure S6) despite the fact that SET1A has an even higher proline density (30 prolines within a 50-aa fragment) than BRD4 (27 out of 50 aa). It is possible that the interaction of PCG with BRD4 not only requires the proline-rich nature of P1 and P2 but also the overall hydrophobicity and the lack of distinctive structures displayed by these sequences are also essential. Future studies are necessary to reveal the precise recognition signature in BRD4 that is explored by PCG to effectively target this protein.

Intrinsically disordered regions (IDRs) are pervasive across eukaryotic proteomes; and in Swiss Protein Database, more than 15,000 proteins are predicted to contain IDRs of greater than 40 amino acids (Romero et al., 1998). IDRs, particularly those containing low complexity sequences, can promote liquid–liquid phase separation (LLPS) through engaging in weak, multivalent interactions (Courchaine et al., 2016). Although the P1 and P2 segments are by definition low-complexity, their deletion from BRD4 did not appear to negatively affect the IDR-mediated phase separation (Figures 4B and 4E). Nevertheless, since P1 and P2 reside in the middle of the BRD4 IDR, by targeting these two segments, PCG was able to efficiently disrupt BRD4 phase separation and convert dynamic nuclear condensates into insoluble aggregates. Our transcriptional analyses indicate that the PCG-induced inhibition of BRD4 LLPS was as effective in suppressing transcription of *MYC* and other BRD4-dependent genes as the JQ1-mediated dissociation of BRD4 from the chromatin templates.

Although LLPS has been shown to play an important role in regulating a diverse and ever-expanding array of biological and pathological processes, the available small molecule tool to inhibit this process so that the contributions of LLPS can be elucidated and LLPS-dependent disease progression can be interrupted is unfortunately very limited. Inhibition of *in vitro* droplet formation or disruption of *in vivo* condensates by 1,6-hexanediol, which is widely used in industrial production of polyester and polyurethane (Kroschwald et al., 2017), has been frequently considered as an indicator of LLPS Molliex et al., 2015; Strom et al., 2017). As expected, this compound was also used to validate the BRD4 IDR-induced LLPS (Cho et al., 2018; Sabari et al., 2018). However, as noted by Alberti et al. (Alberti et al., 2019), 1,6-hexanediol is notoriously non-specific, has no effect on many types of interactions underlying various LLPS cases, and can lead to potential artifacts. In light of this caveat, the identification of PCG as an alternative chemical tool can be used to selectively suppress LLPS formed by BRD4.

Limitations of the study

Our data indicate that the interaction of PCG with BRD4 not only requires the proline-rich nature of the P1 and P2 sequences of BRD4 but also the overall hydrophobicity and the lack of distinctive structures displayed by these sequences are also essential. A major limitation of the current study is that the precise recognition signature in BRD4 that is explored by PCG to effectively target this protein has yet to be determined.

STAR★METHODS

Detailed methods are provided in the online version of this paper and include the following:

- KEY RESOURCES TABLE
- RESOURCE AVAILABILITY
  - Lead contact
  - Materials availability
  - Data and code availability
- EXPERIMENTAL MODEL AND SUBJECT DETAILS
  - Cell lines and culture media
- METHOD DETAILS
  - PCG, antibodies, and plasmids
  - Whole cell extracts preparation and Western blotting
  - Cell proliferation
  - Immunofluorescence staining
  - *In vitro* droplet formation
  - Quantitative RT-PCR analyses
  - ChIP-qPCR
  - Fluorescence recovery after photo bleaching (FRAP)
- QUANTIFICATION AND STATISTICAL ANALYSIS

SUPPLEMENTAL INFORMATION

Supplemental information can be found online at https://doi.org/10.1016/j.isci.2021.103719.

ACKNOWLEDGMENTS

We thank Lu Yi and Li Ran helpful suggestions, discussions, and technical assistance. This work was supported in part by the National Key R&D Program of China (grants 2018YFA0107303& 2020YFA0908100) and the National Natural Science Foundation of China (grants 92053114, 32070632 to H.L. and 81672955 to Y.X.), the Xiamen Southern Oceanographic Center (grant 17GYY002NF02) to X.G., and the National Institutes of Health (grant R01AI41757) to Q.Z.

AUTHORS CONTRIBUTIONS

Conceptualization, C.W., H.L., and Q.Z.; Methodology, C.W., H.L., and Q.Z.; Validation, C.W.; Formal Analysis, C.W.; Investigation, C.W., H.L., and X.L.; Resources, X.G. and W.T.; Writing – Original Draft, C.W., Y.X., and H.C.; Writing – Review & Editing, C.W. and Q.Z.; Funding Acquisition, Y.X., X.G., H.L., and Q.Z.; Supervision, Y.X., H.C., W.T., and Q.Z.

DECLARATION OF INTERESTS

The authors declare no competing interests.

Received: September 29, 2021
Revised: November 22, 2021
Accepted: December 28, 2021
Published: January 21, 2022

REFERENCES

Alberti, S., Gladfelter, A., and Mittag, T. (2019). Considerations and challenges in studying liquid-liquid phase separation and biomolecular condensates. Cell *176*, 419–434. https://doi.org/10.1016/j.cell.2018.12.035.

Bacon, C.W., and D'Orso, I. (2019). CDK9: a signaling hub for transcriptional control. Transcription *10*, 57–75. https://doi.org/10.1080/21541264.2018.1523668.

Bai, L., Zhou, B., Yang, C.Y., Ji, J., McEachern, D., Przybranowski, S., Jiang, H., Hu, J., Xu, F., Zhao, Y., et al. (2017). Targeted degradation of BET proteins in triple-negative breast cancer. Cancer Res. *77*, 2476–2487. https://doi.org/10.1158/0008-5472.CAN-16-2622.

Banerjee, C., Archin, N., Michaels, D., Belkina, A.C., Denis, G.V., Bradner, J., Sebastiani, P., Margolis, D.M., and Montano, M. (2012). BET bromodomain inhibition as a novel strategy for reactivation of HIV-1. J. Leukoc. Biol. *92*, 1147–1154. https://doi.org/10.1189/jlb.0312165.

Bartholomeeusen, K., Xiang, Y., Fujinaga, K., and Peterlin, B.M. (2012). Bromodomain and extra-terminal (BET) bromodomain inhibition activate transcription via transient release of positive transcription elongation factor b (P-TEFb) from 7SK small nuclear ribonucleoprotein. J. Biol. Chem. *287*, 36609–36616. https://doi.org/10.1074/jbc.M112.410746.

Bechter, O., and Schoffski, P. (2020). Make your best BET: the emerging role of BET inhibitor treatment in malignant tumors. Pharmacol.Ther. *208*, 107479. https://doi.org/10.1016/j.pharmthera.2020.107479.

Belkina, A.C., and Denis, G.V. (2012). BET domain co-regulators in obesity, inflammation and cancer. Nat. Rev. Cancer *12*, 465–477. https://doi.org/10.1038/nrc3256.

Cai, D., Lee, A.Y., Chiang, C.M., and Kodadek, T. (2011). Peptoid ligands that bind selectively to phosphoproteins. Bioorg. Med. Chem. Lett. *21*, 4960–4964. https://doi.org/10.1016/j.bmcl.2011.06.011.

Chapuy, B., McKeown, M.R., Lin, C.Y., Monti, S., Roemer, M.G., Qi, J., Rahl, P.B., Sun, H.H., Yeda, K.T., Doench, J.G., et al. (2013). Discovery and characterization of super-enhancer-associated dependencies in diffuse large B cell lymphoma. Cancer Cell *24*, 777–790. https://doi.org/10.1016/j.ccr.2013.11.003.

Chiang, C.M. (2016). Phospho-BRD4: transcription plasticity and drug targeting. Drug Discov. Today Technol. *19*, 17–22. https://doi.org/10.1016/j.ddtec.2016.05.003.

Cho, W.K., Spille, J.H., Hecht, M., Lee, C., Li, C., Grube, V., and Cisse, , II. (2018). Mediator and RNA polymerase II clusters associate in transcription-dependent condensates. Science *361*, 412–415. https://doi.org/10.1126/science.aar4199.

Courchaine, E.M., Lu, A., and Neugebauer, K.M. (2016). Droplet organelles? EMBO J. *35*, 1603–1612. https://doi.org/10.15252/embj.201593517.

Delmore, J.E., Issa, G.C., Lemieux, M.E., Rahl, P.B., Shi, J., Jacobs, H.M., Kastritis, E., Gilpatrick, T., Paranal, R.M., Qi, J., et al. (2011). BET bromodomain inhibition as a therapeutic strategy to target c-Myc. Cell *146*, 904–917. https://doi.org/10.1016/j.cell.2011.08.017.

Devaiah, B.N., Gegonne, A., and Singer, D.S. (2016). Bromodomain 4: a cellular Swiss army knife. J. Leukoc. Biol. *100*, 679–686. https://doi.org/10.1189/jlb.2RI0616-250R.

Ehrnhoefer, D.E., Bieschke, J., Boeddrich, A., Herbst, M., Masino, L., Lurz, R., Engemann, S., Pastore, A., and Wanker, E.E. (2008). EGCG redirects amyloidogenic polypeptides into unstructured, off-pathway oligomers. Nat. Struct. Mol. Biol. *15*, 558–566. https://doi.org/10.1038/nsmb.1437.

Filippakopoulos, P., Qi, J., Picaud, S., Shen, Y., Smith, W.B., Fedorov, O., Morse, E.M., Keates, T., Hickman, T.T., Felletar, I., et al. (2010). Selective inhibition of BET bromodomains. Nature *468*, 1067–1073. https://doi.org/10.1038/nature09504.

Fraga, C.G., Galleano, M., Verstraeten, S.V., and Oteiza, P.I. (2010). Basic biochemical mechanisms behind the health benefits of polyphenols. Mol. Aspects Med. *31*, 435–445. https://doi.org/10.1016/j.mam.2010.09.006.

He, N., Jahchan, N.S., Hong, E., Li, Q., Bayfield, M.A., Maraia, R.J., Luo, K., and Zhou, Q. (2008). A La-related protein modulates 7SK snRNP integrity to suppress P-TEFb-dependent transcriptional elongation and tumorigenesis. Mol.Cell *29*, 588–599. https://doi.org/10.1016/j.molcel.2008.01.003.

Hyman, A.A., Weber, C.A., and Julicher, F. (2014). Liquid-liquid phase separation in biology. Annu. Rev.Cell Dev. Biol. *30*, 39–58. https://doi.org/10.1146/annurev-cellbio-100913-013325.

Jang, M.K., Mochizuki, K., Zhou, M., Jeong, H.S., Brady, J.N., and Ozato, K. (2005). The bromodomain protein Brd4 is a positive regulatory component of P-TEFb and stimulates RNA polymerase II-dependent transcription. Mol.Cell *19*, 523–534. https://doi.org/10.1016/j.molcel.2005.06.027.

Ji, X., Lu, H., Zhou, Q., and Luo, K. (2014). LARP7 suppresses P-TEFb activity to inhibit breast cancer progression and metastasis. Elife *3*, e02907. https://doi.org/10.7554/eLife.02907.

Kress, T.R., Sabo, A., and Amati, B. (2015). MYC: connecting selective transcriptional control to global RNA production. Nat. Rev. Cancer *15*, 593–607. https://doi.org/10.1038/nrc3984.

Kroschwald, S., Maharana, S., and Simon, A. (2017). Hexanediol: a chemical probe to investigate the material properties of membrane-less compartments. Matters, 1–7. https://doi.org/10.19185/matters.201702000010.

Lao-On, U., Rojvirat, P., Chansongkrow, P., Phannasil, P., Siritutsoontorn, S., Charoensawan, V., and Jitrapakdee, S. (2020). c-Myc directly targets an over-expression of pyruvate carboxylase in highly invasive breast cancer. Biochim.Biophys.Acta Mol. Basis Dis. *1866*, 165656. https://doi.org/10.1016/j.bbadis.2019.165656.

Li, Z., Guo, J., Wu, Y., and Zhou, Q. (2013). The BET bromodomain inhibitor JQ1 activates HIV latency through antagonizing Brd4 inhibition of Tat-transactivation. Nucleic Acids Res. *41*, 277–287. https://doi.org/10.1093/nar/gks976.

Lin, Y., Protter, D.S., Rosen, M.K., and Parker, R. (2015). Formation and maturation of phase-separated liquid droplets by RNA-binding proteins. Mol.Cell *60*, 208–219. https://doi.org/10.1016/j.molcel.2015.08.018.

Liu, Z., Wang, P., Chen, H., Wold, E.A., Tian, B., Brasier, A.R., and Zhou, J. (2017). Drug discovery targeting bromodomain-containing protein 4. J. Med. Chem. *60*, 4533–4558. https://doi.org/10.1021/acs.jmedchem.6b01761.

Loven, J., Hoke, H.A., Lin, C.Y., Lau, A., Orlando, D.A., Vakoc, C.R., Bradner, J.E., Lee, T.I., and Young, R.A. (2013). Selective inhibition of tumor oncogenes by disruption of super-enhancers. Cell *153*, 320–334. https://doi.org/10.1016/j.cell.2013.03.036.

Lu, H., Li, Z., Xue, Y., and Zhou, Q. (2013). Viral-host interactions that control HIV-1 transcriptional elongation. Chem. Rev. *113*, 8567–8582. https://doi.org/10.1021/cr400120z.

Lu, H., Yu, D., Hansen, A.S., Ganguly, S., Liu, R., Heckert, A., Darzacq, X., and Zhou, Q. (2018). Phase-separation mechanism for C-terminal hyperphosphorylation of RNA polymerase II. Nature *558*, 318–323. https://doi.org/10.1038/s41586-018-0174-3.

Lu, J., Qian, Y., Altieri, M., Dong, H., Wang, J., Raina, K., Hines, J., Winkler, J.D., Crew, A.P., Coleman, K., and Crews, C.M. (2015). Hijacking the E3 ubiquitin ligase cereblon to efficiently target BRD4. Chem. Biol. *22*, 755–763. https://doi.org/10.1016/j.chembiol.2015.05.009.

Mertz, J.A., Conery, A.R., Bryant, B.M., Sandy, P., Balasubramanian, S., Mele, D.A., Bergeron, L., and Sims, R.J., 3rd (2011). Targeting MYC dependence in cancer by inhibiting BET bromodomains. Proc. Natl. Acad. Sci. U S A. *108*, 16669–16674. https://doi.org/10.1073/pnas.1108190108.

Molliex, A., Temirov, J., Lee, J., Coughlin, M., Kanagaraj, A.P., Kim, H.J., Mittag, T., and Taylor, J.P. (2015). Phase separation by low complexity domains promotes stress granule assembly and drives pathological fibrillization. Cell *163*, 123–133. https://doi.org/10.1016/j.cell.2015.09.015.

Ott, C.J., Kopp, N., Bird, L., Paranal, R.M., Qi, J., Bowman, T., Rodig, S.J., Kung, A.L., Bradner, J.E., and Weinstock, D.M. (2012). BET bromodomain inhibition targets both c-Myc and IL7R in high-risk acute lymphoblastic leukemia. Blood *120*, 2843–2852. https://doi.org/10.1182/blood-2012-02-413021.

Palhano, F.L., Lee, J., Grimster, N.P., and Kelly, J.W. (2013). Toward the molecular mechanism(s) by which EGCG treatment remodels mature amyloid fibrils. J. Am. Chem. Soc. *135*, 7503–7510. https://doi.org/10.1021/ja3115696.

Romero, P., Obradovic, Z., Kissinger, C.R., Villafranca, J.E., Garner, E., Guilliot, S., and Dunker, A.K. (1998). Thousands of proteins likely to have long disordered regions. Pac. Symp.Biocomput. 437–448. https://doi.org/10.3791/2568.

Sabari, B.R., Dall'Agnese, A., Boija, A., Klein, I.A., Coffey, E.L., Shrinivas, K., Abraham, B.J., Hannett, N.M., Zamudio, A.V., Manteiga, J.C., et al. (2018). Coactivator condensation at super-enhancers links phase separation and gene control. Science *361*, eaar3958. https://doi.org/10.1126/science.aar3958.

Schneider, C.A., Rasband, W.S., and Eliceiri, K.W. (2012). NIH Image to ImageJ: 25 years of image analysis. Nat. Methods *9*, 671–675. https://doi.org/10.1038/nmeth.2089.

Shi, J., and Vakoc, C.R. (2014). The mechanisms behind the therapeutic activity of BET bromodomain inhibition. Mol.Cell *54*, 728–736. https://doi.org/10.1016/j.molcel.2014.05.016.

Shu, S., Lin, C.Y., He, H.H., Witwicki, R.M., Tabassum, D.P., Roberts, J.M., Janiszewska, M., Huh, S.J., Liang, Y., Ryan, J., et al. (2016). Response and resistance to BET bromodomain inhibitors in triple-negative breast cancer. Nature *529*, 413–417. https://doi.org/10.1038/nature16508.

Strom, A.R., Emelyanov, A.V., Mir, M., Fyodorov, D.V., Darzacq, X., and Karpen, G.H. (2017). Phase separation drives heterochromatin domain formation. Nature *547*, 241–245. https://doi.org/10.1038/nature22989.

Wang, C., Yang, S., Lu, H., You, H., Ni, M., Shan, W., Lin, T., Gao, X., Chen, H., Zhou, Q., and Xue, Y. (2015). A natural product from polygonum

cuspidatum Sieb. Et Zucc. Promotes Tat-dependent HIV latency reversal through triggering P-TEFb's release from 7SK snRNP. PLoS One *10*, e0142739. https://doi.org/10.1371/journal.pone.0142739.

Williams, S.A., Chen, L.F., Kwon, H., Fenard, D., Bisgrove, D., Verdin, E., and Greene, W.C. (2004). Prostratin antagonizes HIV latency by activating NF-kappaB. J. Biol. Chem. *279*, 42008–42017. https://doi.org/10.1074/jbc.M402124200.

Wu, S.Y., Lee, C.F., Lai, H.T., Yu, C.T., Lee, J.E., Zuo, H., Tsai, S.Y., Tsai, M.J., Ge, K., Wan, Y., and Chiang, C.M. (2020). Opposing functions of BRD4 isoforms in breast cancer. Mol.Cell *78*, 1114–1132 e1110. https://doi.org/10.1016/j.molcel.2020.04.034.

Xu, J., Chen, Y., and Olopade, O.I. (2010). MYC and breast cancer. Genes Cancer *1*, 629–640. https://doi.org/10.1177/1947601910378691.

Yang, Z., Yik, J.H., Chen, R., He, N., Jang, M.K., Ozato, K., and Zhou, Q. (2005). Recruitment of P-TEFb for stimulation of transcriptional elongation by the bromodomain protein Brd4. Mol.Cell *19*, 535–545. https://doi.org/10.1016/j.molcel.2005.06.029.

Zanconato, F., Battilana, G., Forcato, M., Filippi, L., Azzolin, L., Manfrin, A., Quaranta, E., Di Biagio, D., Sigismondo, G., Guzzardo, V., et al. (2018). Transcriptional addiction in cancer cells is mediated by YAP/TAZ through BRD4. Nat. Med. *24*, 1599–1610. https://doi.org/10.1038/s41591-018-0158-8.

Zheng, C.Y., Petralia, R.S., Wang, Y.X., and Kachar, B. (2011). Fluorescence recovery after photobleaching (FRAP) of fluorescence tagged proteins in dendritic spines of cultured hippocampal neurons. J. Vis.Exp. 2568. https://doi.org/10.3791/2568.

Zhou, Q., Li, T., and Price, D.H. (2012). RNA polymerase II elongation control. Annu. Rev. Biochem. *81*, 119–143. https://doi.org/10.1146/annurev-biochem-052610-095910.

Zuber, J., Shi, J., Wang, E., Rappaport, A.R., Herrmann, H., Sison, E.A., Magoon, D., Qi, J., Blatt, K., Wunderlich, M., et al. (2011). RNAi screen identifies Brd4 as a therapeutic target in acute myeloid leukaemia. Nature *478*, 524–528. https://doi.org/10.1038/nature10334.

STAR★METHODS

KEY RESOURCES TABLE

REAGENT or RESOURCE	SOURCE	IDENTIFIER
Antibodies		
AFF1 Antibody	Bethyl Laboratories	Cat# A302-344A
Anti-AFF4 antibody	Abcam	Cat# ab57077
ELL2 Antibody	Bethyl Laboratories	Cat# A302-505A
MEPCE Antibody	Bethyl Laboratories	Cat# A304-184A
CYCT1 antibody	Santa Cruz Biotechnology	Cat# sc-10750
Normal rabbit IgG	Santa Cruz Biotechnology	Cat# sc-2027
Anti-BRD4	Yang et al., 2005	N/A
Anti-LARP7	He et al., 2008	N/A
Anti-HEXIM1	He et al., 2008	N/A
Goat anti-Rabbit IgG (H+L) Superclonal Recombinant Secondary Antibody, Alexa Fluor 488	Life Technologies	Cat# A-27034
Bacterial and virus strains		
E. coli BL21 cells	Lu et al., 2018	N/A
Chemicals, peptides, and recombinant proteins		
CellTiter-Glo2.0® Assay	Promega	Cat# G9242
SYBR Green Mix	Thermo Scientific	Cat#1176202K
KAPA HiFi PCR kit	Roche	Cat# KR0368
Procyanidin C-13,3',3''-tri-O-gallate (PCG)	Wang et al., 2015	N/A
JQ1	Sigma -Aldrich	Cat# SML1524
ARV825	ProbeChem	Cat# PC-45097
EGFP-IDR	This paper	N/A
EGFP-IDR(ΔP1&P2)	This paper	N/A
Experimental models: Cell lines		
HeLa	ATCC	N/A
MDA-MB-231	Ji et al., 2014	N/A
Oligonucleotides		
Primers for qRT-PCR, see Table S1	This paper	N/A
Primers for ChIP-qPCR, see Table S2	This paper	N/A
Recombinant DNA		
Plasmid: pFLAG-CMV2-BRD4 and mutant BRD4(ΔP1&P2, 1-700, 701-1362, 801-1362, 901-1362, 1001-1362, 1101-1362, 1208-1362)	This paper	N/A
Plasmid: pEGFP-BRD4-IDR and BRD4-IDRΔP1&P2	This paper	N/A
Plasmid: EGFP- BRD4-IDR and BRD4-IDRΔP1&P2 (E.coli-based expression)	This paper	N/A
Software and algorithms		
Prism	GraphPad	https://www.graphpad.com/scientific-software/prism/
Image J	Schneider et al., 2012	https://imagej.nih.gov/ij/

RESOURCE AVAILABILITY

Lead contact

Further information and requests for resources and reagents should be directed to and will be fulfilled by the lead contact, Qiang Zhou (qzhou@berkeley.edu).

Materials availability

This study did not generate any new unique reagents. Requests for the constructs should be directed to the laboratory of Professor Qiang Zhou.

Data and code availability

Data reported in this paper will be shared by the lead contact upon request. This paper does not report original code. Any additional information required to reanalyze the data reported in this paper is available from the lead contact upon request.

EXPERIMENTAL MODEL AND SUBJECT DETAILS

Cell lines and culture media

Cell lines used in this study include HeLa (human), MDA-MB-231 (human) (Ji et al., 2014), both of which were cultured in DMEM (Life Technology, 12100061) supplemented with 10% fetal bovine serum. Cells were maintained at 37°C and in the presence of 5% CO_2 in a cell culture incubator.

METHOD DETAILS

PCG, antibodies, and plasmids

Procyanidin C-13,3′,3″-tri-O-gallate, or PCG (previously called as REJ-C1G3(Wang et al., 2015)), was isolated from *Polygonum cuspidatum Sieb.et Zucc.*as described previously (Wang et al., 2015).

Antibodies used in this study are as follows: AFF1 (Bethyl Laboratories, Cat# A302-344A), AFF4 (Abcam, Cat# ab57077), ELL2 (Bethyl Laboratories, Cat# A302-505A), MePCE (Bethyl Laboratories, Cat# A304-184A), CYCT1 (Santa Cruz Biotechnology, Cat# sc-10750), normal rabbit IgG (Santa Cruz Biotechnology, Cat# sc-2027); Anti-BRD4, -LARP7, -HEXIM1 and -CDK9 were generated in our own laboratory and have been described previously(He et al., 2008; Yang et al., 2005).

Plasmids for expressing Flag-tagged WT and mutant BRD4 were constructed in pFLAG-CMV2 vector (Sigma). Plasmids expressing the EGFP fused proteins were constructed by ligating the cDNAs for BRD4-IDR, BRD4-IDRΔP1&P2, BRD4 or BRD4ΔP1&P2 into pEGFP-N1 (Clontech). The *E. coli*-based expression plasmids were generated by inserting the cDNAs encoding BRD4-IDR or BRD4-IDRΔP1&P2 into pGFP-2xStrep (kindly provided by the Hurley lab, UC Berkeley). All plasmids were generated by using KAPA HiFi PCR kit (KR0368, Roche) and the inserts were verified by Sanger sequencing.

Whole cell extracts preparation and Western blotting

Cells were treated under the conditions indicated in the relevant figures and legends, and then collected by centrifugation (1000g, 4°C, 5 min). Cell pellets were washed with ice-cold 1x PBS twice, and lysed for 30 min on ice with the normal cell lysis buffer (1% NP40, 350 mM NaCl, 50 mM Hepes-KOH pH 7.8, 5 mM EDTA, 1 mM DTT, 0.5 mM PMSF) or the normal cell lysis buffer plus 8 M urea. After centrifuge for 10 min at 12,000 g and in 4°C, the supernatant was removed to a new tube as whole cell extracts (WCE or WCE + Urea) for further analysis by Western blotting. For *in vitro* assay, WCE was incubated with the indicated concentrations of PCG at room temperature for 10 min.

All samples for Western analysis were mixed with 4 x SDS loading buffer (200 mM Tris-HCl pH6.8, 400 mM DTT, 8% SDS, 0.4% Bromophenol, 40% Glycerol) in a 3:1 ratio, and boiled for 10 min before analysis by SDS-PAGE followed by standard Western blotting.

Cell proliferation

Cells were seeded in a 96-well plate at a density of 3,000 cells/100 μL (3 wells/sample). After overnight incubation, the cells were treated with the indicated concentrations of PCG or DMSO for 24 hours. CellTiter-Glo2.0 reagent was added to each well containing an equal volume of cell cultural medium present in each

well. The cells were mixed on a shaker for 2 min and incubated at room temperature for 10 min to stabilize the luminescent signal. The recorded fluorescence intensity was calculated by GraphPad Prism.

Immunofluorescence staining

Cells grown on coverslips were fixed at room temperature for 10 min in 4% paraformaldehyde prepared in PBS and then rinsed three times in PBS for 5 min each. The cells were then blocked in 5% normal serum in PBS plus 0.3% Triton X-100 for 60 min. Upon removing the blocking solution, the cells were incubated at 4°C overnight with the indicated primary antibody (1:200) prepared in the blocking solution. After three washes in PBS, the cells were incubated for 60 min at room temperature with the indicated Alexa Fluor-conjugated secondary antibodies (1:1000, Life Technologies) in the blocking solution. After another three washes in PBS, immunofluorescence signals from the stained cells were captured by Zeiss LSM 710 AxioObserver, Zeiss LSM 880 or Zeiss LSM 900 Airyscan2 ZEN blue and ImageJ were used to process images.

In vitro droplet formation

Recombinant EGFP-IDR(WT) and EGFP-IDR(ΔP1&P2) proteins were purified from *E. coli* BL21 cells using the procedure described previously(Lu et al., 2018). Recombinant proteins were expressed *E. coli* BL21 cells in 1L LB medium upon induction overnight with 0.25 mM IPTG at 16°C. Cells were harvested by centrifugation (5000g, 4°C, and 15 min). cell pellets were resuspended in 30 mL lysis buffer (50 mM Tris-HCl pH7.5, 500 mM NaCl, 1 mM DTT, 1% Triton X-100) and lysed by sonication (40% output, 16 cycles of 15 sec on and 15 sec off). The soluble fractions were collected by centrifugation (11,500 rpm, 4°C, 1 hr), and loaded onto the Strep-Tactin column (IBA GmbH). According to protocols provided by the manufacturers, columns was washed with 10 mL washing buffer (20 mM Tris-HCl pH7.5, 500 mM NaCl, 1 mM EDTA, 1% NP-40) for twice. The bound proteins were eluted with 3 mL elution buffer (100 mM Tris-HCl pH7.5, 150 mM NaCl, 1 mM EDTA, 2.5 mM desthiobiotin. The eluted proteins were dialyzed overnight at 4°C against dialysis buffer (150 mM NaCl, 20 mM Tris-HCl pH7.5, 1 mM DTT). Then, the purified proteins were concentrated with Amicon ultra centrifugal filter (Milipore) and stored at −80°C). Purity of the proteins was examined by SDS-PAGE and Coomassie Blue staining and the protein concentrations determined by the Bradford assay.

The droplet formation assay was performed as described previously(Lu et al., 2018). Recombinant proteins were diluted to the indicated concentrations with a buffer containing 20 mM Tris-HCl pH7.5, and 1 mM DTT. 5 μL of the protein solution was added to coverslips and images were acquired by using a Zeiss LSM710 confocal microscope.

Quantitative RT-PCR analyses

The analyses were performed as described previously(He et al., 2008). qRT-PCR reactions were performed with SYBR Green Mix (Thermo Scientific) according to the manufacturer's instructions. All the reactions were done in triplicates. The primers used for the analyses are provided in Table S1. PCR conditions include an initial denaturing step at 94°C for 2 min, and 40 cycles (44 cycles for ChIP-qPCR) of 94°C for 30s and 60°C for 30s. Threshold values (Ct) were calculated to obtain the relative folds of induction.

ChIP-qPCR

Cells grown on 15 cm dishes at 80% confluence were harvested and subjected to the ChIP procedure as described previously(Yang et al., 2005) with the following modifications. Lysed cells were subjected to sonication by using a Covaris-S2 sonicator (Covaris, Inc., Woburn, MA, USA) for a total processing time of 20 min (30 s on and 30 s off). Antibodies used for immunoprecipitation are: 5 μg anti-BRD4 or 5 μg total rabbit IgG. The indicated antibody was incubated with diluted sheared chromatin DNA at 4°C overnight. 20 μL protein A Dynabeads (10003D, Life Technologies) were added to each tube to start the incubation at 4°C for 3 h. The immune complexes were washed once with the low salt immune complex wash buffer (0.1% SDS, 1% Triton X-100, 2 mM EDTA, 20 mM Tris-HCl pH8.1, 150 mM NaCl), once with the high salt immune complex wash buffer (0.1% SDS, 1% Triton X-100, 2 mM EDTA, 20 mM Tris-HCl pH8.1, 500 mM NaCl), once with the LiCl immune complex wash buffer (0.25 M LiCl, 1% NP-40, 1% deoxycholic acid, 1 mM EDTA, 10 mM Tris-HCl pH8.1), twice with the TE buffer (10 mM Tris-HCl pH8.1, 1 mM EDTA), and then eluted with the elution buffer (1% SDS, 500 mM NaHCO3). DNA was purified by using the PCR Purification Kit (Qiagen) and analyzed by quantitative PCR. The sequences of PCR primers used are provided in Table S2.

Fluorescence recovery after photo bleaching (FRAP)

The FRAP assay and data analyses were performed essentially as described(Zheng et al., 2011) with the following modifications. HeLa cells were plated at a density of 60% in a 6-well plate and transfected with the EGFP-IDR(WT) or EGFP-IDR(ΔP1&P2) plasmid (2 μg of each). After 24 h, the transfected cells were plated at a density of 50% in LabTek chambered coverslips (Nunc, Denmark). At 48 h post-transfection, fluorescence images of cells were acquired by a confocal microscope (Zeiss, LSM 710 AxioObserver) equipped with a full incubation chamber maintained in 5% CO2 and at 37°C. Under a 60x oil-immersion objective, a circular spot (radius around 1 μm) was bleached with a laser beam at 100% intensity at 488 nm. Three images as control were acquired before the bleaching. A series of images were captured immediately after bleaching, and then at every 1 sec for 20 sec after bleaching.

To analyze the FRAP data, ImageJ was used for quantification of the fluorescence intensities. First, we calculated the photobleaching rate at each indicated time point (R(t)) by comparing the fluorescence of unbleached region before (Funbleach-pre) and after photobleaching (Funbleach(t)). R(t) = Funbleach(t)/Funbleach-pre. Then we normalized fluorescence intensity: Fbleach-norm(t) = Fbleach(t)/R(t). Finally, we set the normalized fluorescence intensity of pre-bleaching to 100% (Fbleach-norm(pre)), and the normalized fluorescence intensity at each time point was used to calculate the fluorescence recovery (FR): FR(t) = Fbleach-norm(t)/Fbleach-norm(pre). GraphPad Prism was used to plot and analyze the FRAP results(Lin et al., 2015; Molliex et al., 2015), as shown in Figure S2. Single exponential equation: $Y=Y_0 + (Plateau-Y_0) *(1-exp(-K*x))$, where Y_0 is the Yvalue when X (time) is 0. Proportion of recovery is the difference between Y_0 and plateau intensity.

QUANTIFICATION AND STATISTICAL ANALYSIS

Imaging data were quantified by ImageJ (National Institute of Health, Bethesda, MD) (Schneider et al., 2012). Statistical analyses were performed with GraphPad Prism 7 software (GraphPad Software, San Diego, CA). Quantitative real-time PCR, ChIP-qPCR and FRAP data are represented as the mean ± SD. The statistical significance is calculated by two-tailed Student's *t*-test.